Article

Research on Grain Refinement of Sc and Zr Addition in an Al-Mg-Zn Alloy from Experiments and First-Principles Calculations

Tianyou Zhang [1,2,3], Lizhen Yan [1,2,3,*], Xiwu Li [1,2,3,*], Wei Xiao [1,2,3], Guanjun Gao [1,2], Zhihui Li [1,3], Yongan Zhang [1,2,3] and Baiqing Xiong [1,3]

1 State Key Laboratory of Nonferrous Metals and Processes, China GRINM Group Co., Ltd., Beijing 100088, China
2 GRIMAT Engineering Institute Co., Ltd., Beijing 101407, China
3 General Research Institute for Nonferrous Metals, Beijing 100088, China
* Correspondence: yanlizhen@grinm.com (L.Y.); lixiwu@grinm.com (X.L.)

Abstract: The effect of trace Sc and Zr on grain refinement of Al-5.0Mg-3.0Zn as-cast alloy was investigated by optical microscopy and scanning electron microscopy with EDS. The results indicated that the critical quantities of Sc and Zr for Al-Mg-Zn alloy to produce a significant refining effect were determined and the total mass fraction of Sc and Zr was not less than 0.27, and the mass fraction of Sc was more than 0.13. The average grain size of the as-cast alloy ranged from 30 to 44 μm. The as-cast microstructure refinement of the alloy was related to the number density of $Al_3(Sc, Zr)$ particles and the critical nucleation work of grains. Furthermore, based on first-principles calculations, the formation enthalpies of different $Al_3(Sc, Zr)$ particles and the interface stabilities have been theoretically discussed. The experimental phenomenon of increasing the particle number by the simultaneous addition of Sc and Zr was well explained. Thus, this investigation presented a better insight into the grain refining mechanism from experiments and theoretical calculations.

Keywords: Al-Mg-Zn alloy; $Al_3(Sc; Zr)$; grain refinement; casting; first-principles calculations

1. Introduction

Al-Mg-Zn alloy has moderate strength, excellent corrosion resistance and an age-hardening response through precipitating $T-Mg_{32}(Al, Zn)_{49}$ phases and it is expected to be used as structural material in aerospace and various types of hulls [1–5]. It is known that the ingot with fine grains is conducive to improving deformation behaviors and mechanical properties of final products, and microalloying has become one of the main ways to refine the microstructure of alloy grains [6–8]. Sc was found to be an effective alloying element to refine grains by the generation of primary $L1_2-Al_3Sc$ intermetallics in the melt, which provided a heterogeneous nucleation core of α-Al [9]. The equilibrium structure of Al_3Sc is $L1_2$, its lattice constant is 0.4103 nm, and its mismatch with the matrix is 1.32%. However, such effects show up only if Sc addition reaches eutectic composition [10]. Therefore, it is of great significance to add other elements to replace Sc to reduce the cost and further improve the mechanical properties of the alloy due to the high price of Sc. Er, Hf, Yb and Zr can be identified as elements similar to Sc, which can dissolve in phase $L1_2$ and improve its thermal stability [11]. However, the lattice constants of Al_3Er and Al_3Yb are 0.4215 nm and 0.4202 nm, and the mismatches with the matrix are 4.08% and 3.71%. Moreover, the solid solubility of Er and Yb in aluminum is far less than that of Sc [12,13]. The lattice constant of Al_3Hf is almost the same as that of aluminum, which is 0.4048 nm and the mismatch with the matrix is 0.04%. However, the diffusion coefficient of Hf is very small, which is not conducive to the precipitation of Al_3Hf [14]. At present, the common approach is to replace Sc with the Zr element. Zr has a lower diffusion coefficient than Sc, which can effectively improve the thermal stability and the mismatch between Al_3Zr, and the matrix is only 0.75% [15–17]. On the other hand, the primary $Al_3(Sc, Zr)$ particles can obviously refine the as-cast microstructure and improve the strength and formability of the alloy [18–20].

Owing to the great contribution of grain refinement, numerous investigations on the $Al_3(Sc, Zr)$ primary particles found in aluminum alloys have been carried out [19,21]. Pan [19] studied the effect of Sc and Zr on the microstructure of as-cast Al-5Mg alloy. The results indicated that 0.2 wt.% Sc did not produce a grain refining effect but eliminated the dendrite substructure of Al-5Mg alloy. When the Sc content reached 0.6 wt.%, the average grain size decreased from 265.1 μm to 50.3 μm. The average grain size decreased to 54.6 μm when 0.2 wt.% Sc and 0.1 wt.% Zr were added. Moreover, the Al_3Sc phase could be identified as the eutectics consisted of Al_3Sc and α-Al phases, which exhibited an 'Al_3Sc + α-Al + Al_3Sc' multilayer structure [22]. The same result was found in Al-6Mg alloy [10]. For Al-Zn-Mg-Cu series alloys, adding 0.20% Zr or 0.20% Sc can partially refine the grains in Al-7.2Zn-2.2Mg-1.8Cu alloy, while adding 0.10% Sc + 0.20% Zr can obviously refine the grains, and the average grain size was only 15 μm [21]. Based on three-dimensional electron backscatter diffraction, Li [23,24] observed layer upon layer of growth of $Al_3(Sc, Zr)$. Al, Cu, Si and Fe were enriched between the α-Al matrix and the cellular eutectic $Al_3(Sc, Zr)$ phase, while Sc, Ti and Zr were enriched in the fine $Al_3(Sc, Zr)$ phase. Xu [25] suggested that the primary $Al_3(Sc, Zr)$ particles had different morphological characteristics due to the different cooling rates, but all the particles exhibited an obvious $Al_3Sc/Al_3(Sc, Zr)$ core-shell structure.

On the other hand, theoretical calculations based on density functional theory were a good way to understand the grain refinement mechanism. In the framework of the edge-edge (E2E) matching model, the grain refinement of aluminum by Al_3Zr and Al_3Sc primary particles can be well explained from the perspective of lattice mismatch [26]. Clouet [9] built an atomic kinetic model for Al-Zr and Al-Sc binary systems so as to be as close as possible to the real systems. The model can be used to simulate the precipitation kinetics of Al_3Zr and Al_3Sc at an atomic scale. The combination of first-principles calculations and experiments can effectively investigate the refining mechanism of primary $Al_3(Sc, Zr)$ particles. The current research focuses on the microalloying of Sc and Zr in Al-Mg and Al-Zn-Mg-Cu series alloys, focusing on the morphology, size and precipitation process of the primary phase, as well as the effect on the refinement of the as-cast microstructure. At present, there are few studies on the effect of Sc and Zr contents on the critical point of microstructure refinement in as-cast Al-Mg-Zn alloys.

In the present work, a comparative experiment was designed to investigate the effects of single and compound addition of Sc and Zr on the as-cast microstructure of Al-5.0Mg-3.0Zn alloy, and the main novelty of this study is the determination of critical quantities of Sc and Zr for Al-Mg-Zn alloys to produce significant refining results. Moreover, the refining mechanism of Sc and Zr in Al-Mg-Zn alloys has been studied based on phase diagram and first-principles calculations. This work helps us to understand grain refining mechanism in Al-Mg-Zn alloys, which provide guidance for industrial production.

2. Experimental Section

2.1. Experimental Procedures

The nominal compositions of the alloys are listed in Table 1. The raw materials were 99.99%Al, pure zinc, pure magnesium and Al-2wt.%Sc, Al-5wt.%Zr and Al-10wt.%Mn. Firstly, raw materials were melted in an electrical resistance furnace. Then, the molten melt was poured at 720 °C into a cylindrical iron plate mold with a height of 50 mm and a radius of 60 mm, then the ingots were air-cooled to room temperature. Specimens for further investigation were cut from the center of the ingot. The first set of experiments investigated the effect of adding Sc and Zr separately on the as-cast microstructure. Then, the effect of the Sc content on the as-cast microstructure was studied when 0.1 wt.% Zr content was added. In order to further explore the effect of Sc and Zr content on grain refinement, the third set of experiments explored the effect of the Sc to Zr ratio on the as-cast microstructure.

Table 1. Composition of the alloy (wt.%).

Group Number	Alloy No.	Mg	Zn	Mn	Sc	Zr
	Base alloy	5.0	3.0	0.5	0	0
I: single addition of Sc or Zr	0.27Sc	5.14	3.0	0.5	0.27	0
	0.27Zr	5.1	3.0	0.5	0	0.27
	0Sc-0.1Zr	5.1	2.93	0.54	0	0.1
	0.1Sc-0.1Zr	4.99	2.89	0.54	0.1	0.1
II: addition of Sc only if mass fraction of Zr was 0.1	0.15Sc-0.1Zr	4.98	3.0	0.5	0.15	0.1
	0.17Sc-0.1Zr	5.12	3.04	0.48	0.17	0.1
	0.2Sc-0.1Zr	5.0	3.02	0.5	0.2	0.1
	0.07Sc-0.2Zr	5.0	3.0	0.52	0.07	0.20
III: different Sc to Zr ratio only if the total mass fraction of Sc and Zr was 0.27	0.1Sc-0.17Zr	5.12	3.02	0.5	0.1	0.17
	0.13Sc-0.14Zr	4.98	3.0	0.5	0.13	0.14
	0.2Sc-0.07Zr	5.0	3.0	0.5	0.20	0.07

The metallographic samples were divided into two groups. The first one was anode coating after being electropolished and then the grain size of the cast alloy was observed by OM (Optical Microscope). The composition ratio of the anode coating solution was 38 mL H_2SO_4, 43 mL H_3PO_4 and 19 mL deionized water per 100 mL. Pictures were taken with an optical microscope after the film was coated. Grain size analysis was carried out using the linear intercept method with at least 10 pictures. The microstructure of the second batch of samples was analyzed by JEOL JSM 7001F (JEOL, Tokyo, Japan) field emission scanning electron microscope. The equipment was equipped with an Energy Dispersive Spectrometer (EDS, JEOL, Tokyo, Japan) module, which accelerates the electrical voltage of 20~25kV. Pandat developed by CompuTherm LLC (Pandat 2022, CompuTherm LLC, TEXAS, USA) was used for phase diagram calculation.

2.2. DFT Calculation Details

All calculations in this work were performed by first-principles methods based on density functional theory (DFT), as implemented in Vienna Ab-inito Simulation Package (VASP, version 6.1, University of Vienna, Vienna, Germany) code. The generalized gradient approximation (GGA) parameterized by Perdew, Burke and Ernzerhof (PBE) was used to describe the exchange-correlation function. A plane-wave energy cut-off of 500 eV was set in all calculations, and the calculations of unit cells were performed using Monkhorst-Pack *k*-point meshes of $12 \times 12 \times 12$. The energy tolerance was set to be 1.0×10^{-5} eV and the force tolerance was 1.0×10^{-4} eV Å^{-1}.

Al_3Sc, Al_3Zr and $Al_3(Sc, Zr)$ are the same crystal structure as Cu_3Al(cubic) and belong to the space group $L1_2$ (Pm-3 m) at room temperature. Each Al atom is located in the center of four Sc (Zr) atoms in the four-atom primitive cell, as presented in Figure 1. The corresponding positions are as follows: Sc (Zr) at (0, 0, 0) and Al at (0, 1/2, 1/2: 1/2, 0, 1/2: 1/2, 1/2, 0) [27,28].
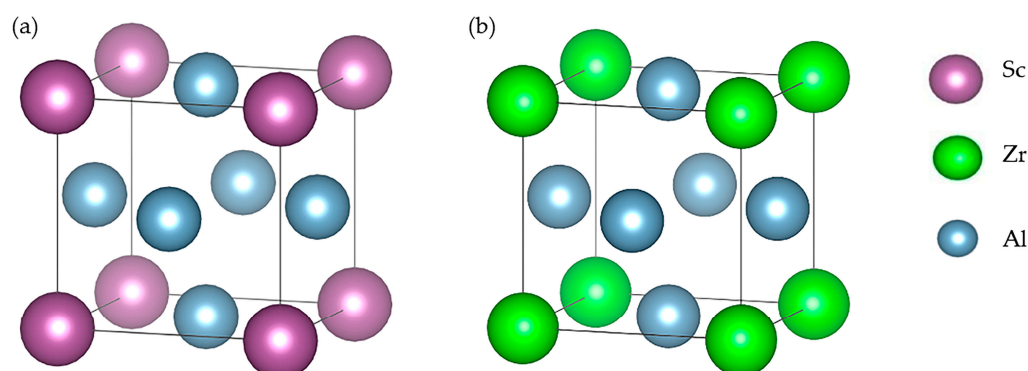
Figure 1. Crystal models of $L1_2$-Al_3Sc and $L1_2$-Al_3Zr. (**a**) $L1_2$-Al_3Sc, (**b**) $L1_2$-Al_3Zr.

In order to deeply analyze the thermodynamic stabilities of $Al_3(Sc, Zr)$, different supercells were constructed by doping Sc into Al_3Zr. Considering the different Sc/Zr ratios

and atomic occupancies, we used the Pymatgen software package (version 3.7, Materials Virtual Lab, La Jolla, CA, USA) to seek the atomic configurations and performed systematic calculations to find the most stable doping structures. Based on these, 30 $Al_3(Sc, Zr)$ models with different doping sites were constructed, and three models with the lowest energy in $2 \times 2 \times 2$ and $2 \times 2 \times 4$ supercells were selected for the following studies. Figure 2 shows the structures of $Al_3(Sc, Zr)$ for different doping systems.

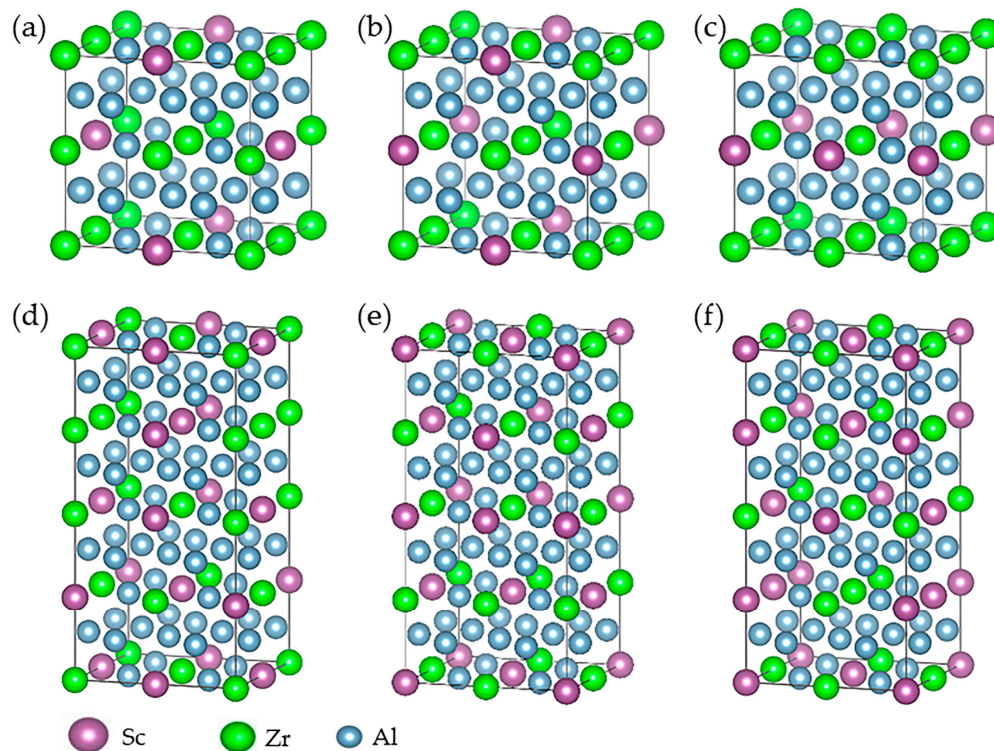**Figure 2.** Crystal models of $Al_3(Sc, Zr)$ for different doping systems. (**a**) $Al_{24}Sc_2Zr_6$-1; (**b**) $Al_{24}Sc_2Zr_6$-2; (**c**) $Al_{24}Sc_2Zr_6$-3; (**d**) $Al_{48}Sc_8Zr_8$-1; (**e**) $Al_{48}Sc_8Zr_8$-2; (**f**) $Al_{48}Sc_8Zr_8$-3.

3. Results and Discussions

3.1. Grain Refinement of Sc and Zr Addition in Al-Mg-Zn Alloys

The grain structure of as-cast alloys is shown in Figure 3. The as-cast microstructure exhibited a typical dendritic substructure within coarse grains only if there was a single addition of Sc or Zr. It was observed in Figure 3b,c that the grain size was slightly modified by the addition of 0.27 wt.% Sc or 0.27 wt.% Zr. The results indicated that the grain refinement was very weak. Figure 4 presents the average grain size of Al-Mg-Zn alloy with the single addition of Sc and Zr. It was observed that the grain size of Al-Mg-Zn without a trace element (Figure 3a) was 297 μm, while the average grain size was 197 μm with adding 0.27 wt.% Sc (Figure 3b), and the alloy with adding 0.27 wt.% Zr (Figure 3c) was 260 μm. It can be suggested that the addition of 0.27 wt.% Zr did not result in grain refinement significantly. So, the single addition of Sc has a better grain refining effect compared to the addition of Zr. However, for the coarse structure of the alloy with 0.27 wt.% Sc, the addition of 0.27 wt.% Sc content was still not enough to form primary Al_3Sc particles in the melt, although the existence of Mg and Zn was found to decrease the solubility of scandium in solid solution [29], which supported the results of this study. Therefore, the grain was not obviously refined with the single addition of Sc or Zr. Then, we studied the grain structure of as-cast alloys by adding Sc and Zr simultaneously.
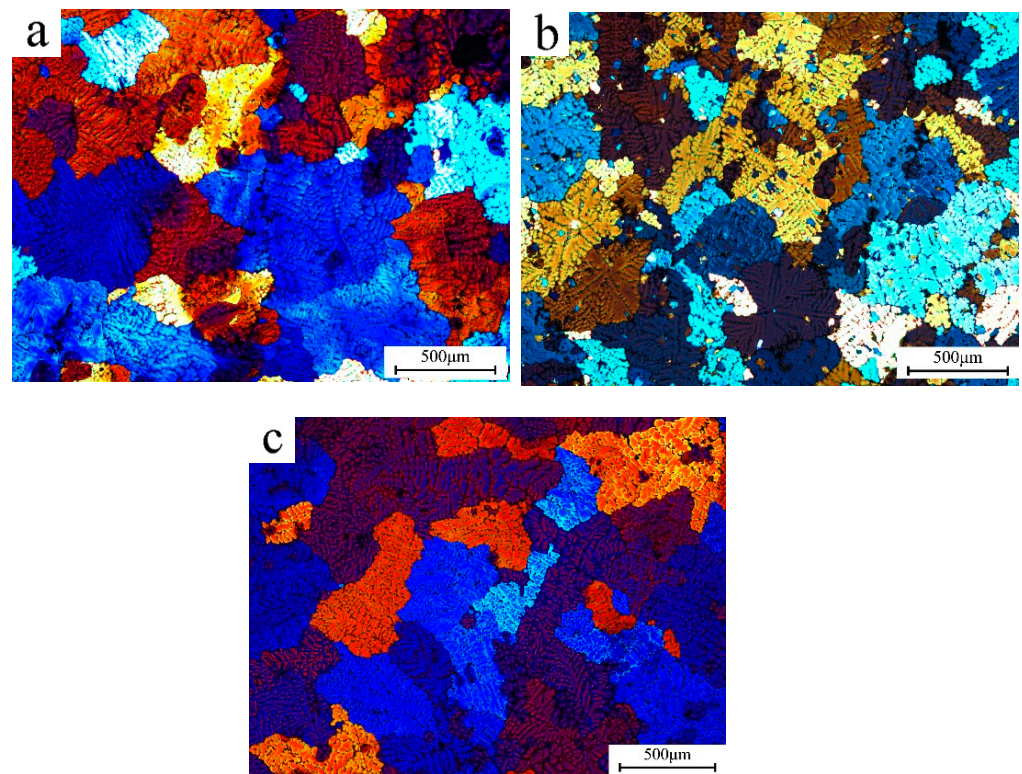
Figure 3. As-cast microstructures of Al-Mg-Zn alloy: (**a**) 0Sc-0Zr; (**b**) 0.27Sc-0Zr; (**c**) 0Sc-0.27Zr.
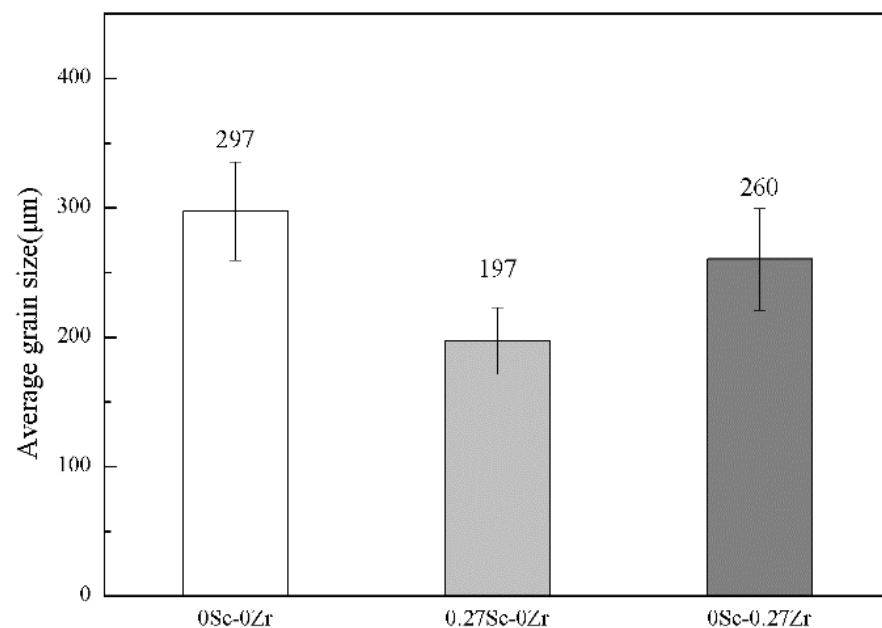

Figure 4. Average grain size of Al-Mg-Zn alloy with single addition of Sc and Zr element.

The grain structure of as-cast alloys with Sc and 0.1 wt.% Zr is shown in Figure 5. The dendritic substructure with coarse grain was obvious in the alloys of 0 wt.% Sc, 0.1 wt.% Sc and 0.15 wt.% Sc (Figure 5a–c), whereas the equiaxed structure was found in the alloy with 0.17 wt.% Sc and 0.20 wt.% Sc (Figure 5d,e). The as-cast grains were refined significantly while the mass percentage of Sc was less than 0.17. Figure 6 displays the evolution of the average grain size, calculated using the standard linear intercept method. The average grain sizes of as-cast alloy with 0 wt.% Sc, 0.1 wt.% Sc and 0.15 wt.% Sc were 169, 192 and 191 μm, respectively. The results showed that the grain refinement degree was weak

when adding a low content of Sc and Zr elements. This was probably because there are not enough cores formed in the melt to refine the grains. However, the average grain sizes of as-cast alloy with 0.17 wt.% Sc and 0.20 wt.% Sc ranged from 30 to 33 μm. This indicated that with the increase of the Sc content, the average grain size decreased further, so that the benefit of grain refinement was greater. It was easy to see that when the total mass fraction of Sc and Zr was not less than 0.27, the as-cast structure of the alloy was obviously refined. Thus, we studied the grain structure of as-cast alloys with different Sc to Zr ratios while the total mass percentage of Sc and Zr was 0.27.
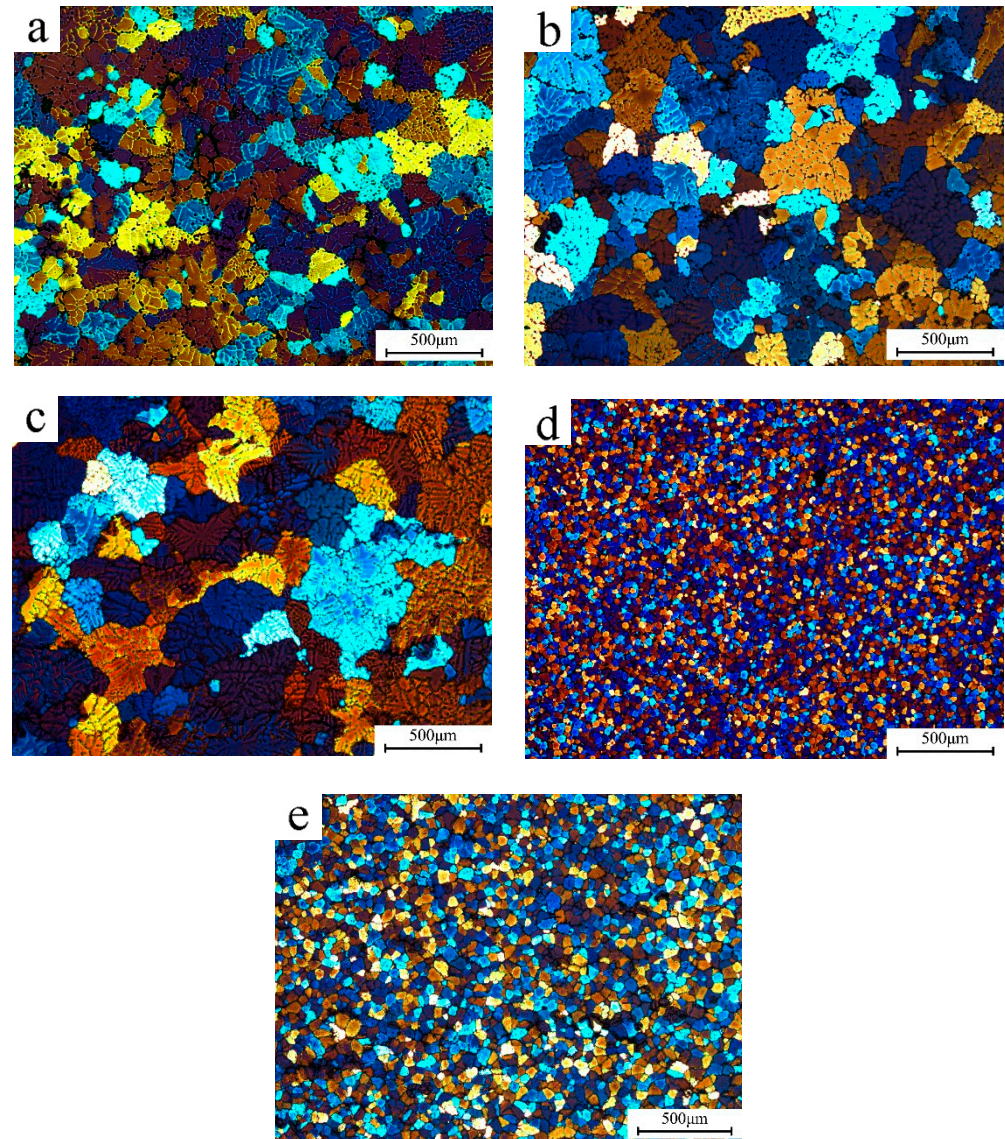
Figure 5. As-cast microstructures of Al-Mg-Zn alloy with different Sc content: (**a**) 0Sc-0.10Zr; (**b**) 0.10Sc-0.10Zr; (**c**) 0.15Sc-0.10Zr; (**d**) 0.17Sc-0.10Zr; (**e**) 0.20Sc-0.10Zr.

The grain structure of as-cast alloys with different Sc to Zr ratios while the total mass fraction of Sc and Zr was 0.27 is shown in Figure 7. The as-cast grains were refined with a Sc to Zr ratio ranging from 0.9 to 2.9, whereas the as-cast alloy exhibited coarse grains in which the Sc to Zr ratio was less than 0.6. Figure 8 shows the evolution of the average grain size. The average grain size of the as-cast alloy ranged from 150 to 165 μm when the Sc to Zr ratio was 0.35 and 0.6, respectively. In contrast, when the Sc to Zr ratio was more than 0.9, the as-cast grains can be significantly reduced even at a lower Zr level, in which the average grain size was between 30 and 44 μm. According to the above results, the grain

refinement effect of the composite addition of Sc and Zr was higher than that of the single addition of Sc or Zr. Meanwhile, the composite addition of Sc and Zr can effectively reduce costs. Considering the cost factor, we considered the alloy with 0.13 wt.% Sc and 0.14 wt.% Zr as a typical alloy for the study.
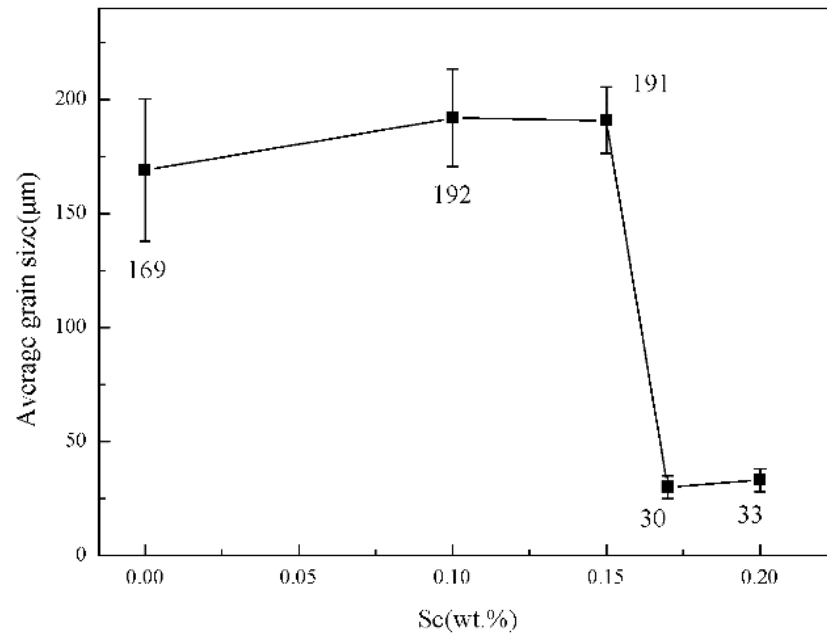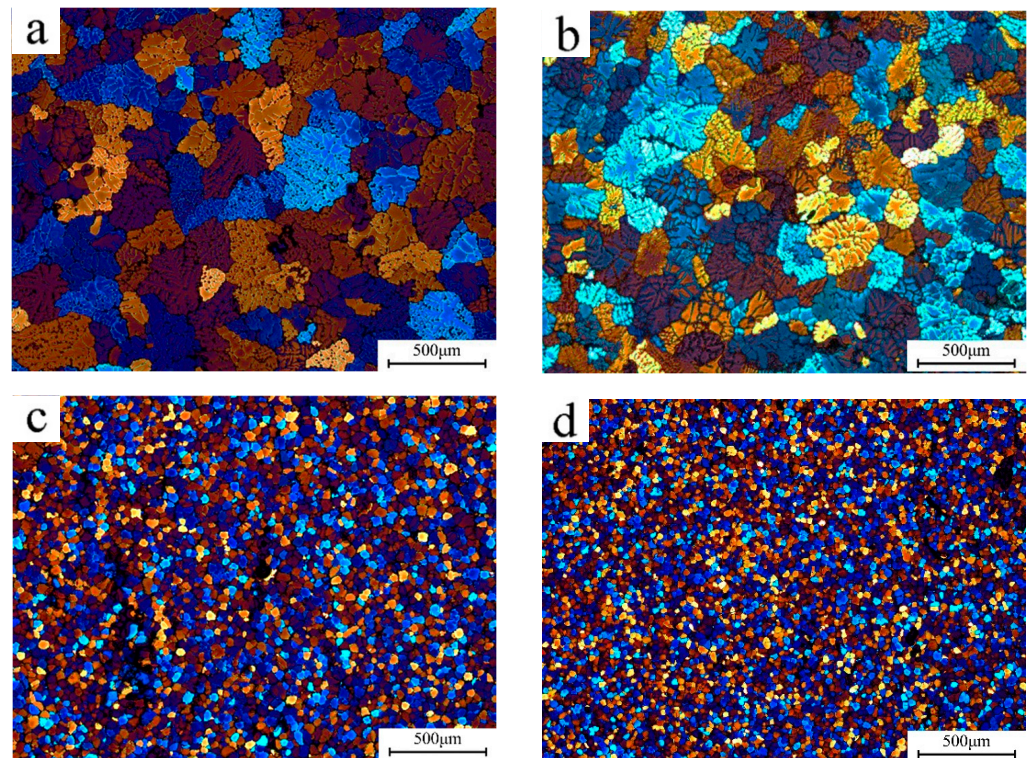

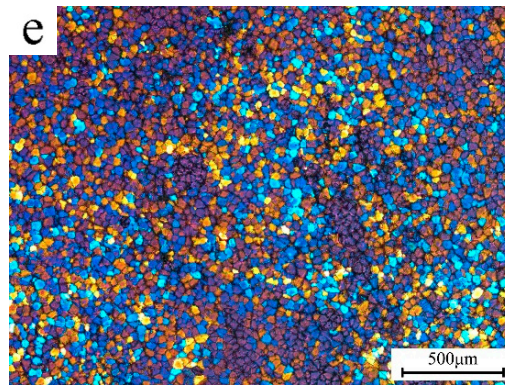**Figure 6.** Average grain size of Al-Mg-Zn alloy with addition of 0.1 wt.% Zr.

Figure 7. *Cont.*

Figure 7. As-cast microstructures of Al-Mg-Zn alloy with different Sc to Zr ratios: (**a**) 0.07Sc-0.20Zr; (**b**) 0.1Sc-0.17Zr; (**c**) 0.13Sc-0.14Zr; (**d**) 0.17Sc-0.10Zr; (**e**) 0.20Sc-0.07Zr.
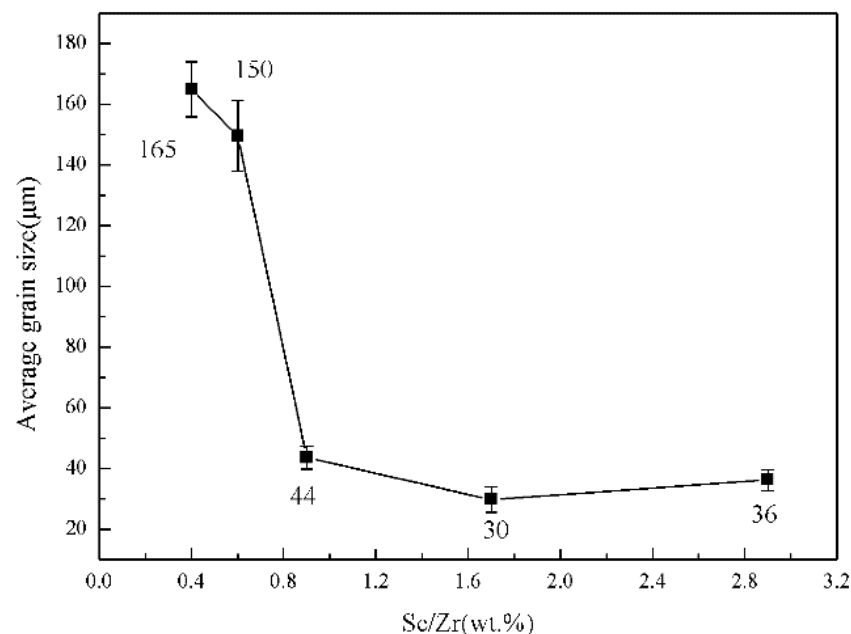

Figure 8. Average grain size of Al-Mg-Zn alloy with different Sc to Zr ratios.

3.2. Intermetallics of as-Cast Al-Mg-Zn Alloys

The microstructure of as-cast alloy was studied using a scanning electron microscope (SEM), and the influence of Sc and Zr addition to the alloy was investigated. We selected the base alloy, the alloy with 0.07 wt.% Sc and 0.20 wt.% Zr (grains not refined significantly) and alloy with 0.13 wt.% Sc and 0.14 wt.% Zr (grains refined significantly) as the research objects. Figure 9 presents the second phase of the base alloy (Figure 9a,b) and the alloy with 0.07 wt.% Sc and 0.20 wt.% Zr. The EDS results are shown in Table 2. In the terms of SEM observations and EDS results, the T-$Al_6Mg_{11}Zn_{11}$ phase (bright contrast) was along grain boundaries in the α-Al (fcc) matrix (dark contrast). There were some massive white Mn-rich phases in the base alloy. However, Al_3(Sc, Zr) phase was not observed in the as-cast alloy.

Figure 10 shows the SEM images of the second phase of the alloy with 0.13 wt.% Sc and 0.14 wt.% Zr. The EDS results are displayed in Table 3. In particular, there were some flocculent and honeycomb second phases along the grain boundary and within the grain in the alloy. This phase could be identified as Al_3(Sc, Zr). It was generally located at the grain boundary and combined with the Fe-Mn-rich phase and T phase. Pan [19] found two different morphologies of primary Al_3(Sc, Zr) particles in Al-Mg alloy, including square and triangular features, and all the particles possessed a similar multilayer structural feature.

Xu [25] observed the morphology of primary particles of Al-Sc-Zr alloy at different cooling rates. The results showed that the primary $Al_3(Sc, Zr)$ particles were small cubic, pointed cubic or cross-flower-shaped particles at a slow cooling rate. The primary particles were separated in a crisscross shape at a moderate cooling rate and in a sharp cubic shape at a high cooling rate. The reason why the $Al_3(Sc, Zr)$ phase was flocculent and honeycomb in this experiment needs to be further explored.

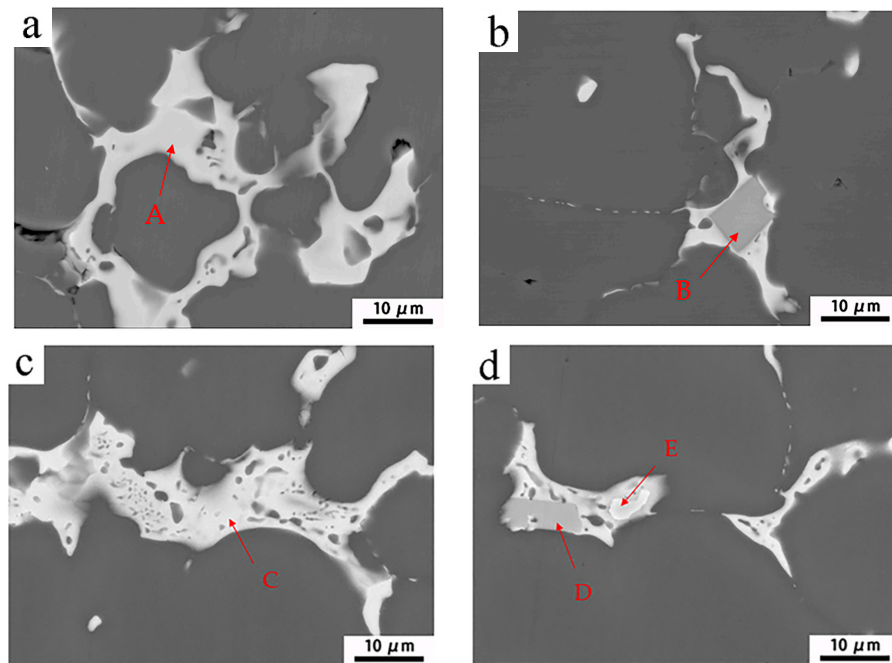**Figure 9.** SEM image of second phase in alloy: (**a**,**b**) base alloy; (**c**,**d**) 0.07Sc-0.20Zr alloy.
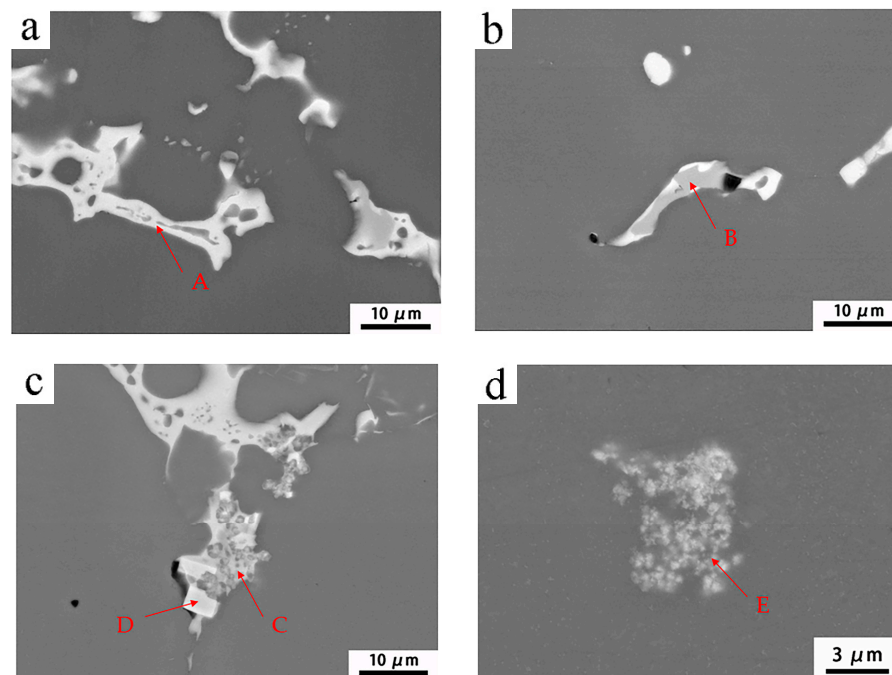
Figure 10. SEM image of second phase in alloy with 0.13 wt.% Sc and 0.14 wt.% Zr. (**a**) T phase, (**b**) Mn-rich phase, (**c**,**d**) $Al_3(Sc, Zr)$ phase.

Table 2. EDS spectrum analysis results of the intermetallic marked in Figure 9 (at.%).

Element	Al	Mg	Zn	Mn	Fe
A	48.4	37.5	14.1	-	-
B	73.2	15.0	3.8	8.0	-
C	47.4	38.5	14.1	-	
D	75.7	5.8	1.4	3.5	
E	77.7	3.8	1.5	7.0	10.0

Table 3. EDS spectrum analysis results of the intermetallic marked in Figure 10 (at.%).

Element	Al	Mg	Zn	Mn	Fe	Sc	Zr
A	58.6	27.3	14.1	-		-	-
B	70.9	15.3	4.6	9.3		-	
C	75.7	5.8	1.4	3.5		9.1	3.7
D	75.1	4.3	1.2	12.5	7.3	-	-
E	88.1	4.6	1.3	-		4.7	1.4

In order to further clarify the complex structure, primary particle samples showing more details of microstructure were selected for study, and the results are shown in Figure 11. From the results of line scan elements analysis, it can be seen that the primary $Al_3(Sc, Zr)$ phase had a layered structure of "$Al_3(Sc, Zr) + Al + Al_3(Sc, Zr)$" from two-dimensional space observation, which was similar to the experimental results reported by Forbord [30].
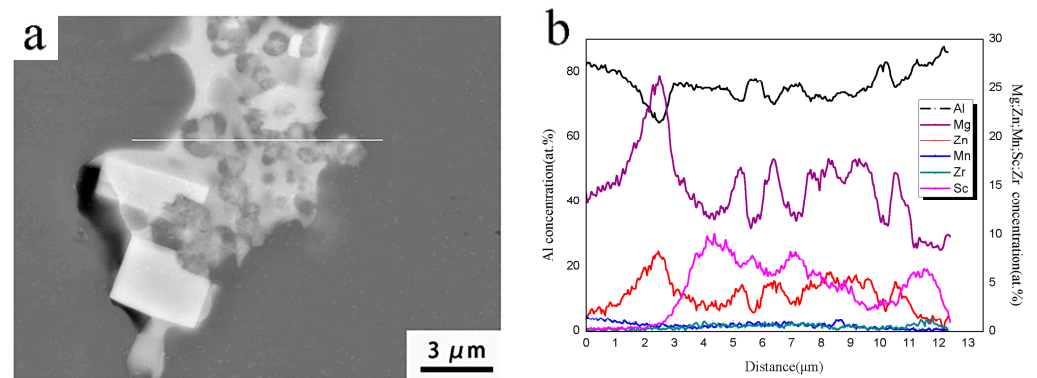
Figure 11. SEM images and line scan elements analysis (LSEA) of particles extracted from samples. (**a**) $Al_3(Sc, Zr)$ phase, (**b**) line scanning of $Al_3(Sc, Zr)$.

4. Discussion

Considering the difference in the actual casting process, the grain size of Al-5.0Mg-3.0Zn alloy was divided into three gradients. The grain size of the base alloy was 300 µm; after adding Sc and Zr, the grain size was between 150 to 200 µm. When the total mass fraction of Sc and Zr was not less than 0.27, and the mass fraction of Sc was more than 0.13, the as-cast grains can be significantly refined, and the average grain size ranged from 20 to 40 µm. Figure 12 shows the formation of $Al_3(Sc, Zr)$ during solidification. Al_3Zr particles were formed firstly under a temperature above 650 °C. Once peritectic particles (Al_3Zr) were formed, further solidification was controlled by a peritectic reaction to form an Al layer: $Al_3Zr + liquid \rightarrow Al$. The Al layer can be used as the nucleation surface of the initial eutectic reaction: liquid$\rightarrow \alpha$-Al+Al_3Sc [23]. This is owing to the very close orientation relationship and very small lattice mismatch between Al (fcc, a = 0.4050 nm) and Al_3Sc ($L1_2$, a = 0.4105 nm), which promoted the nucleation of Al_3Sc on Al. However, Wang [21] suggested that the Al_3Zr nucleated preferentially; then, Al_3Sc was covered at the surface of Al_3Zr particles. Finally, $Al_3(Sc, Zr)$ particles with a layered structure were formed. The next step was α-Al nucleation by $Al_3(Sc, Zr)$ particles. Although there was some controversy, it was recognized that Al_3Zr particles formed firstly during the solidification process.

Figure 13 presents the phase diagram calculation results of Al-5.0Mg-3.0Zn-0.5Mn-xZr with a different Sc content. With the increase of the Zr content, the formation temperature of Al_3Zr particles increased, and there were more Al_3Zr particles in the melt. According to the SEM results, the as-cast microstructure can only be refined effectively if the $Al_3(Sc, Zr)$ particles existed in the alloy. Taking the alloy with 0.07 wt.% Sc and 0.20 wt.% Zr as an example, the Al_3Zr particles precipitated firstly in the melt, then the α-Al matrix was formed by the peritectic reaction ($Al_3Zr + L \rightarrow$ α-Al) at 630 °C. The Fe-Mn-rich phase began to precipitate at 580 °C until the solidification ended at 550 °C. In the whole solidification process, only the Al_3Zr particles served as the nucleating point to fine the microstructure, so the influence on the grain size was not obvious. But for the alloy with 0.13 wt.% Sc and 0.14 wt.% Zr, Al_3Zr still formed initially, and Al_3Sc particles precipitate at 600 °C, then $Al_3(Sc, Zr)$ particles with layered composite structure formed. The experimental study indicated that Al_3Zr was more stable than Al_3Sc, and $Al_3(Sc, Zr)$ phases were more likely to precipitate and stabilize than Al_3Zr and Al_3Sc [19,30–32]. Next, we will discuss the effect of Al_3Sc, Al_3Zr and $Al_3(Sc, Zr)$ particles on the as-cast grain structure of Al-Mg-Zn alloy.
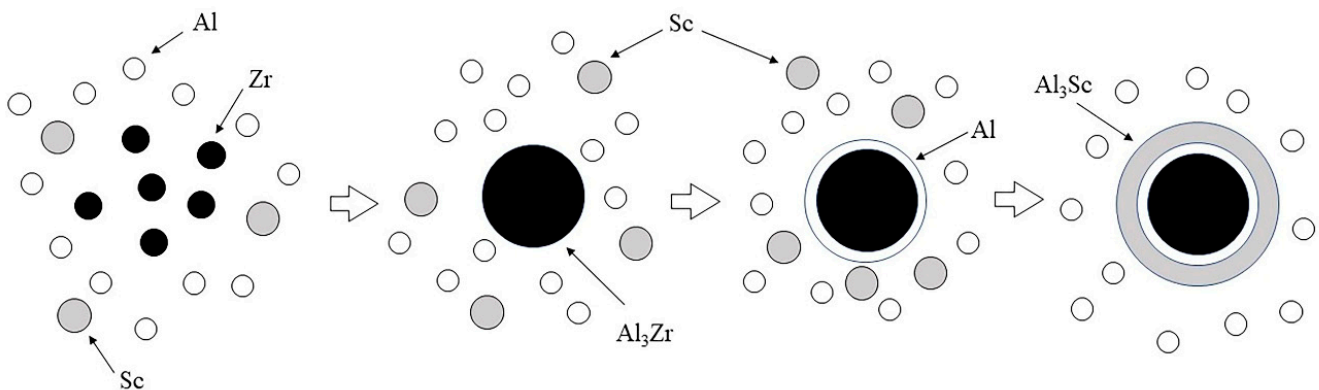

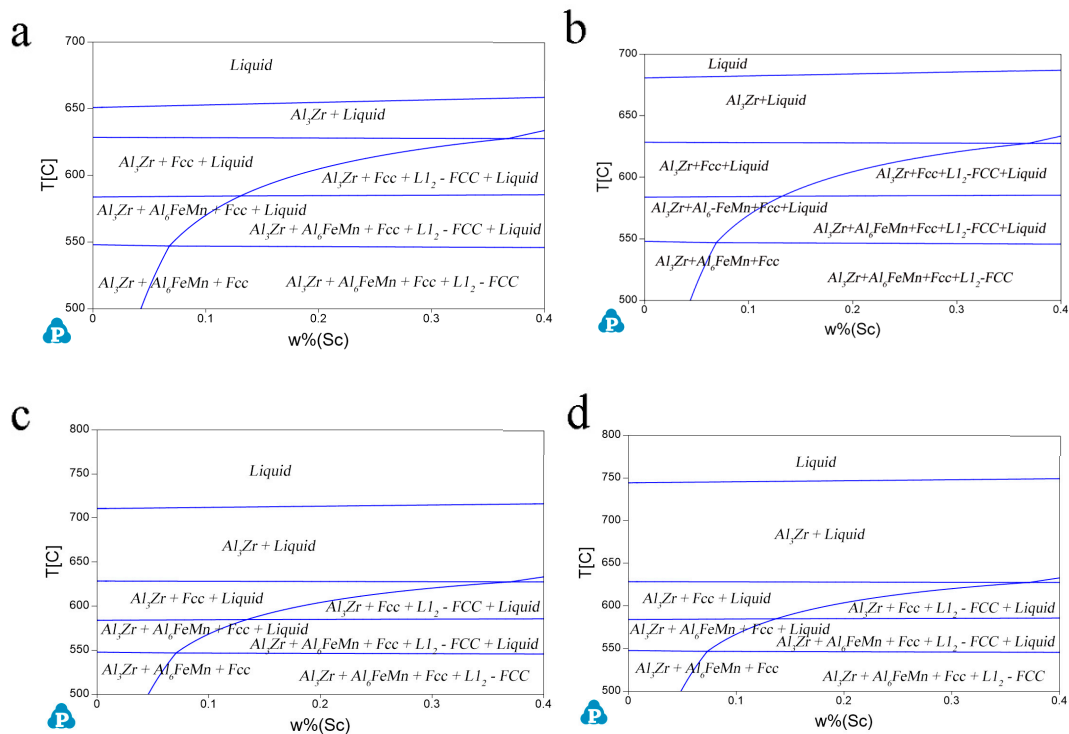**Figure 12.** Formation process of primary $Al_3(Sc, Zr)$ phase.

Figure 13. Phase diagram calculation results of Al-5.0Mg-3.0Zn-0.5Mn-xZr alloy with different Sc content: (**a**) 0.07Zr; (**b**) 0.1Zr; (**c**) 0.14Zr; (**d**) 0.20Zr.

Accordingly, the calculated lattice parameters of Al_3Sc and Al_3Zr are summarized in Table 4 and compared with the values from other sources. As clearly presented, the calculated lattice parameters of Al_3Sc and Al_3Zr are in good agreement with other works and experimental results [33–36]. The lattice misfit of Al_3Sc with Al is a little lower than Al_3Zr, which implies that the interfacial energy of Al_3Sc/α-Al could be lower than that of Al_3Zr/α-Al.

Table 4. The calculated lattice parameters for Al_3Sc, Al_3Zr and $Al_3(Sc, Zr)$ and the lattice misfit with Al.

Systems	Lattice Parameter (Å)	Lattice Misfit (%)
Al	4.05	-
	4.103	1.304
Al_3Sc	4.106 [34]	-
	4.047 [33]	-
	4.105	1.361
Al_3Zr	4.113 [35]	-
	4.117 [36]	-
$Al_{24}Sc_2Zr_6$-1	4.098	1.361
$Al_{24}Sc_2Zr_6$-2	4.096	1.185
$Al_{24}Sc_2Zr_6$-3	4.097	1.132
$Al_{48}Sc_8Zr_8$-1	4.097	1.161
$Al_{48}Sc_8Zr_8$-2	4.096	1.161
$Al_{48}Sc_8Zr_8$-3	4.105	1.146

To understand the dependence of different doping sites on lattice parameters in supercell, we calculated the lattice parameters of $Al_3(Sc, Zr)$ at different Sc/Zr ratios, and calculated the corresponding lattice mismatch between Al and $Al_3(Sc, Zr)$. The obtained results are also presented in Table 4. It can be seen that with the change of the Sc/Zr ratio, the lattice parameter of $Al_3(Sc, Zr)$ and the lattice mismatch with Al also changes. Obviously, the lattice misfit between $Al_3(Sc, Zr)$ and Al is very low, only 1.13 to 1.36%, and it decreases with the increase in the Sc content. Therefore, it can be deduced that the interface energy of Sc-doped Al/Al_3Zr was reduced, and the interface of $Al/Al_3(Sc, Zr)$ could be more stable than Al/Al_3Zr. Thus, the stability of Al/Al_3Zr interfaces can be strengthened with Sc doping. Li [33] has also reported that the addition of the Sc element is beneficial to the formation of the interface, improving the bonding strength and wetting effect of the interface, which is consistent with our results. It can be well explained that Sc doping can reduce the lattice mismatch between Al and Al_3Zr, which is responsible for the grain refinement of Al-Mg-Zn alloy.

The number density of nucleated particles is related to the enthalpy of formation. Table 5 shows the enthalpies of formation and bond orders of Al_3Sc, Al_3Zr and $Al_3(Sc, Zr)$ with different Sc to Zr ratios. Both the formation enthalpy and bond order depict the strength of the atomic bonding in the crystal, reflecting the stability of the compound. The higher the bond order, the stronger the bond. The formation enthalpies of Al_3Zr and $Al_3(Sc, Zr)$ particles are almost equal, which means that these compounds are easier to precipitate than Al_3Sc during solidification. This is consistent with the result of phase diagram calculations. For the solidification stage, the larger formation enthalpy can lead to more particle precipitation, which is beneficial to improve the properties of the alloy. The bond orders for different systems are also listed in Table 4. Bond orders for the Al-Zr bond (~0.32) are always larger than that of Al-Sc bonds (~0.23), which represents the stronger covalent binding between Al and Zr atoms. With the increase in Sc content, the Al-Zr bond orders in $Al_3(Sc, Zr)$ particles also increase. For Sc-Zr bonds, their bond strengths are very weak with only ~0.015 bond orders. Previous studies [33] have also shown that the formation enthalpy of $Al_3(Sc, Zr)$ is lower than that of Al_3Sc phases. Therefore, due to the small interfacial mismatch and strong thermodynamic stability of $Al_3(Sc, Zr)$, the simultaneous addition of Sc and Zr into Al alloys might be beneficial to the grain refinement.

Table 5. The calculated enthalpies of formation and bond orders for Al_3Sc, Al_3Zr and $Al_3(Sc, Zr)$ in different systems.

Systems	Enthalpy of Formation (kJ/mol)	Bond	Bond Order
Al_3Sc	−18.96	Al-Sc	0.236
Al_3Zr	−19.57	Al-Zr	0.318
$Al_{24}Sc_2Zr_6$-1	−20.07	Al-Sc	0.231
		Al-Zr	0.314
		Sc-Zr	0.015
$Al_{24}Sc_2Zr_6$-2	−19.88	Al-Sc	0.234
		Al-Zr	0.323
		Sc-Zr	0.015
$Al_{24}Sc_2Zr_6$-3	−19.88	Al-Sc	0.236
		Al-Zr	0.320
		Sc-Zr	0.015
$Al_{48}Sc_8Zr_8$-1	−19.59	Al-Sc	0.239
		Al-Zr	0.328
		Sc-Zr	0.016
$Al_{48}Sc_8Zr_8$-2	−19.97	Al-Sc	0.234
		Al-Zr	0.323
		Sc-Zr	0.015
$Al_{48}Sc_8Zr_8$-3	−19.97	Al-Sc	0.236
		Al-Zr	0.324
		Sc-Zr	0.015

5. Conclusions

The critical values of Sc and Zr content refining Al-5.0Mg-3.0Zn alloys were investigated by comparative experiments, and the grain refining mechanism was investigated from both experimental and first-principles calculations and the main conclusions were drawn as follows.

(1) The content of Sc and Zr had a significant effect on the as-cast structure of Al-Mg-Zn alloy. The critical content of Sc and Zr which can produce a remarkable refining effect on Al-Mg-Zn alloy was that the total mass fraction of Sc and Zr was not less than 0.27, and the mass fraction of Sc was more than 0.13. The average grain size ranged from 30 to 44 μm.

(2) A primary $Al_3(Sc, Zr)$ phase existed in the remarkably refined alloy, which was honeycomb and flocculent, and there was no primary $Al_3(Sc, Zr)$ phase in the as-alloy with coarse grains.

(3) The lattice misfit of Al/Al_3Zr was higher than that of Al/$Al_3(Sc, Zr)$, which indicated that the $Al_3(Sc, Zr)$ phase can serve as a better heterogeneous nucleation for α-Al for its lower interface energy.

(4) The formation energy of the $Al_3(Sc, Zr)$ was lower than that of the Al_3Sc phase. This meant that the nucleation driving force of $Al_3(Sc, Zr)$ was beneficial to the refinement phase. Thus, the alloy with 0.13 wt.% Sc and 0.14 wt.% Zr was refined significantly.

Author Contributions: Conceptualization, T.Z. and L.Y.; methodology, T.Z.; software, W.X.; validation, T.Z., G.G. and L.Y.; formal analysis, T.Z.; investigation, Y.Z.; resources, B.X.; data curation, B.X.; writing—original draft preparation, T.Z.; writing—review and editing, T.Z.; visualization, Z.L.; supervision, X.L.; project administration, X.L.; funding acquisition, L.Y. All authors have read and agreed to the published version of the manuscript.

Data Availability Statement: No new data were created or analyzed in this study. Data sharing is not applicable to this article.

Conflicts of Interest: The authors declare no conflict of interest.

References

1. Meng, C.; Zhang, D.; Cui, H.; Zhuang, L.; Zhang, J. Mechanical properties, intergranular corrosion behavior and microstructure of Zn modified Al–Mg alloys. *J. Alloys Compd.* **2014**, *617*, 925–932. [CrossRef]
2. Hou, S.; Liu, P.; Zhang, D.; Zhang, J.; Zhuang, L. Precipitation hardening behavior and microstructure evolution of Al-5.1Mg-0.15Cu alloy with 3.0Zn (wt%) addition. *J. Mater. Sci.* **2018**, *53*, 3846–3861.
3. Takata, N.; Ishihara, M.; Suzuki, A.; Kobashi, M. Microstructure and strength of a novel heat-resistant aluminum alloy strengthened by T-Al6Mg11Zn11 phase at elevated temperatures. *Mater. Sci. Eng. A* **2018**, *739*, 62–70. [CrossRef]
4. Meng, C.; Zhang, D.; Zhuang, L.; Zhang, J. Correlations between stress corrosion cracking, grain boundary precipitates and Zn content of Al-Mg-Zn alloys. *J. Alloys Compd. Interdisc. J. Mater. Sci. Solid-State Chem. Phys.* **2016**, *655*, 178–187. [CrossRef]
5. Liu, T.W.; Wang, Q.D.; Tang, H.P.; Li, Z.Y.; Chuan, L.E.I.; Ebrahimi, M.; Jiang, H.Y.; Ding, W.J. Microstructure and mechanical properties of squeeze-cast Al−5.0 Mg−3.0 Zn−1.0 Cu alloys in solution-treated and aged conditions. *Trans. Nonferrous Met. Soc. China* **2020**, *30*, 2326–2338. [CrossRef]
6. El-Danaf, E.; Soliman, M.; Almajid, A.; El-Rayes, M. Enhancement of mechanical properties and grain size refinement of commercial purity aluminum 1050 processed by ECAP. *Mater. Sci. Eng. A* **2007**, *458*, 226–234. [CrossRef]
7. Ebrahimi, M.; Attarilar, S.; Gode, C.; Djavanroodi, F. Damage prediction of 7025 aluminum alloy during equal-channel angular pressing. *Int. J. Miner. Met. Mater.* **2014**, *21*, 990–998. [CrossRef]
8. Jung, S.S.; Son, Y.G.; Park, Y.H.; Lee, Y.C. A Study on the Grain Refining Mechanisms and Melt Superheat Treatment of Aluminum-Bearing Mg Alloys. *Metals* **2022**, *12*, 464. [CrossRef]
9. Clouet, E.; Nastar, M.; Sigli, C. Nucleation of Al$_3$Zr and Al$_3$Sc in aluminum alloys: From kinetic Monte Carlo simulations to classical theory. *Phys. Rev. B* **2004**, *69*, 064109. [CrossRef]
10. Kaiser, M.S.; Datta, S.; Roychowdhury, A.; Banerjee, M.K. Effect of scandium on the microstructure and ageing behaviour of cast Al-6Mg alloy. *Mater. Charact.* **2008**, *59*, 1661–1666. [CrossRef]
11. Mochugovskiy, A.G.; Barkov, R.Y.; Mikhaylovskaya, A.V.; Loginova, I.S.; Yakovtseva, O.A.; Pozdniakov, A.V. Structure and Properties of Al–4.5 Mg–0.15 Zr Compo-sitions Alloyed with Er, Y, and Yb. *Phys. Met. Metallogr.* **2022**, *123*, 466–473. [CrossRef]
12. Gschneidner, K.A.; Calderwood, F.W. The Al−Er (Aluminum-Erbium) system. *Bull. Alloy. Phase Diagr.* **1988**, *9*, 676–678. [CrossRef]
13. Gschneidner, K.A.; Calderwood, F.W. The Al-Yb (aluminum-ytterbium) system. *Bull. Alloy. Phase Diagr.* **1989**, *10*, 47–49. [CrossRef]
14. Murray, J.L.; McAlister, A.J.; Kahan, D.J. The Al-Hf (aluminum-hafnium) system. *J. Phase Equilibria Diffus.* **1998**, *19*, 376. [CrossRef]
15. Fuller, C.B.; Murray, J.L.; Seidman, D.N. Temporal evolution of the nanostructure of Al$_3$(Sc, Zr) alloys: Part I–Chemical compositions of Al$_3$(Sc1−xZrx) precipitates. *Acta Mater.* **2005**, *53*, 5401–5413. [CrossRef]
16. Fuller, C.B.; Seidman, D.N. Temporal evolution of the nanostructure of Al$_3$(Sc, Zr) alloys: Part II-coarsening of Al$_3$ (Sc1−x Zrx) precipitates. *Acta Mater.* **2005**, *53*, 5415–5428. [CrossRef]
17. Sun, F.; Nash, G.L.; Li, Q.; Liu, E.; He, C.; Shi, C.; Zhao, N. Effect of Sc and Zr additions on microstructures and corrosion behavior of Al-Cu-Mg-Sc-Zr alloys. *J. Mater. Sci. Technol.* **2017**, *33*, 1015–1022. [CrossRef]
18. Norman, A.; Prangnell, P.; McEwen, R. The solidification behaviour of dilute aluminium–scandium alloys. *Acta Mater.* **1998**, *46*, 5715–5732. [CrossRef]
19. Pan, D.; Zhou, S.; Zhang, Z.; Li, M.; Wu, Y. Effects of Sc(Zr) on the microstructure and mechanical properties of as-cast Al–Mg alloys. *Mater. Sci. Technol.* **2017**, *33*, 751–757. [CrossRef]
20. Zhou, S.; Zhang, Z.; Li, M.; Pan, D.; Su, H.; Du, X.; Li, P.; Wu, Y. Correlative characterization of primary particles formed in as-cast Al-Mg alloy containing a high level of Sc. *Mater. Charact.* **2016**, *118*, 85–91. [CrossRef]
21. Wang, Z.G.; Xu, J.; Li, B.; Zhang, Z.F. Study on Refinement Mechanism of Sc and Zr as-cast Al-7.2 Zn-2.2 Mg-1.8 Cu alloys. In *Applied Mechanics and Materials*; Trans Tech Publications Ltd.: Stafa-Zurich, Switzerland, 2013.
22. Zhou, S.; Zhang, Z.; Li, M.; Pan, D.; Su, H.; Du, X.; Li, P.; Wu, Y. Effect of Sc on microstructure and mechanical properties of as-cast Al–Mg alloys. *Mater. Des.* **2015**, *90*, 1077–1084. [CrossRef]
23. Li, J.; Wiessner, M.; Albu, M.; Wurster, S.; Sartory, B.; Hofer, F.; Schumacher, P. Correlative characterization of primary Al$_3$(Sc, Zr) phase in an Al–Zn–Mg based alloy. *Mater. Charact.* **2015**, *102*, 62–70. [CrossRef]
24. Li, J.H.; Oberdorfer, B.; Wurster, S.; Schumacher, P. Impurity effects on the nucleation and growth of primary Al$_3$(Sc,Zr) phase in Al alloys. *J. Mater. Sci.* **2014**, *49*, 5961–5977. [CrossRef]
25. Cong, X.U.; Rou, D.U.; Wang, X.J.; Hanada, S.; Yamagata, H.; Wang, W.H. Effect of cooling rate on morphology of primary particles in Al-Sc-Zr master alloy. *Trans. Nonferrous Met. Soc. China* **2014**, *24*, 2420–2426.
26. Zhang, M.X.; Kelly, P.M.; Easton, M.A.; Taylor, J.A. Crystallographic study of grain refinement in aluminum alloys using the edge-to-edge matching model. *Acta Mater.* **2005**, *53*, 1427–1438. [CrossRef]
27. Sun, S.; Li, X.; Wang, H.; Jiang, H.; Lei, W.; Jiang, Y.; Yi, D. First-principles investigations on the electronic properties and stabilities of low-index surfaces of L1$_2$–Al$_3$Sc intermetallic. *Appl. Surf. Sci.* **2013**, *288*, 609–618. [CrossRef]
28. Yang, T.; Han, X.; Ding, Z.; Wang, Y.; Li, J. Electronic and structural properties of low-index L1$_2$–Al$_3$Zr surfaces by first-principle calculations. *Calphad* **2019**, *66*, 101645. [CrossRef]
29. Wen, S.P.; Xing, Z.B.; Huang, H.; Li, B.L.; Wang, W.; Nie, Z.R. The effect of erbium on the microstructure and mechanical properties of Al–Mg–Mn–Zr alloy. *Mater. Sci. Eng. A* **2009**, *516*, 42–49. [CrossRef]

30. Forbord, B.; Lefebvre, W.; Danoix, F.; Hallem, H.; Marthinsen, K. Three dimensional atom probe investigation on the formation of Al$_3$(Sc, Zr)-dispersoids in aluminium alloys. *Scr. Mater.* **2004**, *51*, 333–337. [CrossRef]

31. Knipling, K.E.; Karnesky, R.A.; Lee, C.P.; Dunand, D.C.; Seidman, D.N. Precipitation evolution in Al–0.1 Sc, Al–0.1 Zr and Al–0.1 Sc–0.1 Zr (at.%) alloys during isochronal aging. *Acta Mater.* **2010**, *58*, 5184–5195. [CrossRef]

32. Li, S.-S.; Li, L.; Han, J.; Wang, C.-T.; Xiao, Y.-Q.; Jian, X.-D.; Qian, P.; Su, Y.-J. First-Principles study on the nucleation of precipitates in ternary Al alloys doped with Sc, Li, Zr, and Ti elements. *Appl. Surf. Sci.* **2020**, *526*, 146455. [CrossRef]

33. Chunmei, L.; Xianquan, J.; Nanpu, C.; Jianfeng, T.; Zhiqian, C. First-principles Investigation on Formation Energy, Elasticity and Interfacial Properties of Refining Phase Al-3 (Zr, Sc) in Al Alloys. *Rare Met. Mater. Eng.* **2020**, *49*, 2557–2566.

34. Zhang, C.; Jiang, Y.; Cao, F.; Hu, T.; Wang, Y.; Yin, D. Formation of coherent, core-shelled nano-particles in dilute Al-Sc-Zr alloys from the first-principles. *J. Mater. Sci. Technol.* **2019**, *35*, 930–938. [CrossRef]

35. Liu, Y.; Zhang, C.-C.; Zhang, X.-Y.; Huang, Y.-C. Understanding grain refinement of Sc addition in a Zr containing Al-Zn-Mg-Cu aluminum alloy from experiments and first-principles. *Intermetallics* **2020**, *123*, 106823. [CrossRef]

36. Zhang, C.; Yin, D.; Jiang, Y.; Wang, Y. Precipitation of L12-phase nano-particles in dilute Al-Er-Zr alloys from the first-principles. *Comput. Mater. Sci.* **2019**, *162*, 171–177. [CrossRef]